Hydro-mechanical modeling of a vegetated slope subjected to rainfall

Hamed Sadeghi[1*], *Farshad* Yazdani Bene Kohal[1], *Mostafa* Gholami[1], *Pouya* Alipanahi[1], and *Dongri* Song[2]

[1] Department of Civil Engineering, Sharif University of Technology, Tehran, Iran
[2] Institute of Mountain Hazards and Environment, Chinese Academy of Sciences, Chengdu, Sichuan, China

Abstract. Shallow landslides triggered by heavy rainfalls have caused casualties and economic losses to domestic infrastructures and industries worldwide. Rainfall mainly reduces the soil matric suction and the shear resistance, resulting in shallow landslides. Vegetation is an eco-friendly and cost-effective method for stabilizing slopes prone to shallow landslides. This research aims to investigate the hydrological and mechanical effects of vegetation on slope stability through a numerical study approach. Vegetated and bare slopes were subjected to a recorded climate condition and two rainfall scenarios of high intensity (HI) and low intensity (LI). Matric suction and factor of safety of vegetated and bare slopes subjected to rainfall were investigated. The matric suction of the vegetated slope at the surface was approximately four times greater than the bare slope after the HI scenario. However, the matric suction is about three times greater in the LI scenario. The results indicate that planting on slopes would reduce the vulnerability of bare slopes to the HI rainfall due to the higher matric suction and additional cohesion induced by the root system. These findings suggest that using vegetation in Rasht, Iran, where the climate data were collected, has considerable potential for stabilizing slopes.

1 Introduction

Geoengineering concerns over the stability of unsaturated slopes have grown considerably over the past few years [1-3]. Landslides are a major concern worldwide, leading to many social and economic losses [4]. Therefore, taking preventive measures and reducing human societies' damage by landslides is one of the primary challenges [5, 6].

There are different solutions to deal with shallow landslides caused by rainfall. Soil nailing, anchoring systems, and geosynthetics are generally used for slope stabilization [7]. But these methods are expensive and harmful to the environment. Vegetation as an eco-friendly and cost-effective method to stabilize shallow landslides has been widely used in recent decades.

The presence of vegetation due to its hydrological and mechanical effects causes slope stabilization [5, 8-10]. From a hydrological point of view, plant transpiration due to root water uptake reduces the volumetric water content in the soil and increases the matric suction [5, 11-13]. The increase in matric suction and hence the enhancement of shear strength causes the stability of slopes [14, 15]. The stability of slopes depends on hydraulic conductivity. The roots of the plants by occupying soil pores and releasing root exudate, decreases hydraulic conductivity [11, 16-20]. On the other hand, the presence of vegetation may increase hydraulic conductivity due to the decay of roots [11], and the creation of preferential flow paths[21, 22]. Therefore, depending on conditions such as planting density, plant species, and plant age, hydraulic conductivity may increase or decrease[11, 23].

In addition, roots enhance the mechanical properties of the soil. There are two approaches being established to quantify the mechanical effects of vegetation. In the first approach, roots in the soil create a composite material that increases soil cohesion. In the second approach, the root-soil interactions are simulated by using the physical mechanisms that contribute to soil strength [8].

Various numerical studies were conducted to simulate vegetation and its effect on hydraulic and mechanical properties. The impact of vegetation on slope displacement subjected to rainfall [24, 25], different species of vegetation on slope stability [9], the density of the vegetated soil [26], temperature and humidity on matric suction [27], and variability in root length in slope stability [28], have been investigated following the numerical approach. However, considering of hydraulic and mechanical properties of the soils are still lacking.

The main goal of this research is to investigate slope stability with and without vegetation. To achieve that, through vegetation modeling, the effect of vegetation on the hydraulic and mechanical properties of the soil has been considered. A tree species, Schefflera heptaphylla, is used for slope stability. Two slopes are modeled with the same geometry and the same boundary conditions. Matric suction changes and factors of safety in two different rainfall scenarios are investigated.

2 Materials and methods

A parametric study was conducted to investigate the effects of vegetation on the soil and the stability of the slopes in the GeoStudio software package. The slope condition is initially in steady state condition for a short time. When the rainfall starts, the transient state analysis is performed. At the same time, the stability of the slope is calculated. An extended Mohr-Coulomb equation can

* Corresponding author: hsadeghi@sharif.edu

be used to calculate the shear strength of unsaturated soil [29].

$$\tau_f = c' + (\sigma_n - u_a)\tan\phi' + (u_a - u_w)[\tan\phi'(\frac{\theta_w - \theta_r}{\theta_s - \theta_r})] \quad (1)$$

where c′ is the soil cohesion (kPa); σ_n is the net stress (kPa); φ′ is the friction angle; u_a is pore air pressure; (u_a-u_w) is the matric suction where u_w is pore-water pressure; θ_r is the residual volumetric water content; and θ_s is the saturated volumetric water content. The Morgenstern-Price method has been used to determine the slope's safety factor. It should be noted that the factor of safety were calculated for the critical slip surface.

2.1 Climate input data

The selected climate data are related to Rasht, Iran, from 2020 to 2021. The climate conditions of Rasht are similar to those of tropical areas. Fig. 1 shows the maximum and average rainfall of rainy days per month. Maximum rainfall per month varied from 0 to 80 mm/day, and average rainfall of rainy days per month varied from 0 to 20 mm/day.

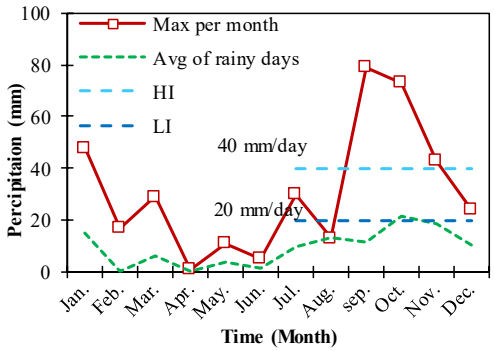

Fig. 1. Annual variations of the maximum and average rainfall of rainy days per month

Accordingly, two rainfall scenarios were chosen: a high-intensity rainfall scenario (HI scenario) based on maximum rainfall and a low-intensity rainfall scenario (LI scenario) based on average rainfall on rainy days. In both scenarios, the total amount of rainfall applied to the model is 400 mm. Table 1 summarizes the details of two rainfall scenarios considered in this study.

Table 1. Details of simulated rainfall scenarios

Scenario	Rainfall intensity (mm/day)	Duration of rainfall (day)	Total amount of rainfall (mm)
HI*	40	10	400
LI*	20	20	

* HI; High intensity , LI; Low intensity

Fig. 2 shows the solar radiation and temperature variations for a year. Solar radiation and temperature fluctuated from 6.5 to 17.5 Mj/day/m^2 and 10 to 28℃, respectively. The average solar radiation flux of 12 Mj/day/m^2 and temperature average of 18℃ were chosen as shown in Fig. 2 The humidity of this region was generally high, and the average humidity during the year was 85%. The annual average wind speed was 0.173 m/s.

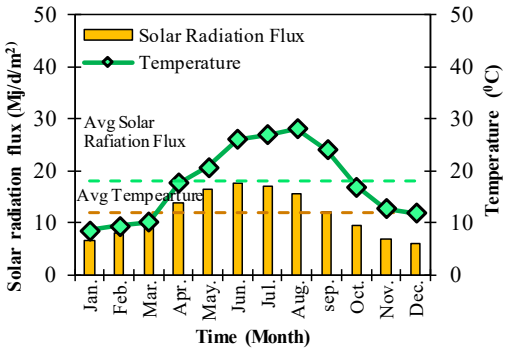

Fig. 2. Annual fluctuations of solar radiation and temperature

According to these climate data, the evapotranspiration was calculated using the Penman-Monteith equation expressed as:

$$q_{PET} = \frac{1}{h_{fg}}\left[\frac{\Gamma(q_n - q_g)}{\Gamma + \gamma(1 + \frac{r_c}{r_a})} + \frac{\frac{\rho_a c_{sa}(p_{v0}^a - p_v^a)}{r_a}}{\Gamma + \gamma(1 + \frac{r_c}{r_a})}\right] \quad (2)$$

where h_{fg} is the latent heat of vaporization (MJ/kg), q_n is the net radiation (Mj/day/m^2), q_g is ground heat flux (Jm^2/d), ρ_a is mean air density (kg/m^3), c_{sa} is the specific heat moist air (J/kg/°C), p_{v0} is the saturated vapor pressure at mean air temperature (kPa), p_v is the actual air vapor pressure at the reference height (kPa), r_c is the bulk surface resistance (s/m), and r_a is the aerodynamic resistance (s/m).

2.2 Plant properties

The plant species in this study is Schefflera heptophylla, which is compatible with the mentioned region and widely used due to its ability of drought tolerant and control of soil erosion. Various parameters of this plant for modeling were retrieved from the experimental literature for the planting density of 180 mm [12]. Due to the consideration of plant growth and actual conditions during analyzing, Table 2 shows a summary of the properties of the plant during four months.

Table 2. Properties of the Schefflera heptophylla [12]

	First month	After 4 months of growth
Leaf area index	1.6	6.2
Root depth, mm	83	157
Vegetation height, mm	440	573

The maximum possible transpiration rate is depended on the soil moisture. The presence of wet conditions causes oxygen deficiency, and the presence of dry conditions limits water availability. As a result of the factors mentioned above, the actual transpiration

value is lower than the maximum value. Therefore, the actual transpiration rate equation is as follows [30]:

$$T = \alpha_{rw}\pi'_{root}q_{PT} \quad (3)$$

where α_{rw} is the normalized transpiration rate due to water stress, π'_{root} the normalized water uptake distribution, and the potential transpiration flux.

Fig. 3 shows the normalized transpiration rate of Schefflera heptophylla, which is varied from 0.0 to 1.0. Transpiration rate is the ability of the plant to take water around the root zone according to soil suction [13]. According to Fig. 3, The transpiration rate is 1.0, up to 100 kPa suction. Beyond this particular suction, the plant's transpiration rate decreases until it reaches the wilting point, which at this point, the transpiration rate reaches zero.

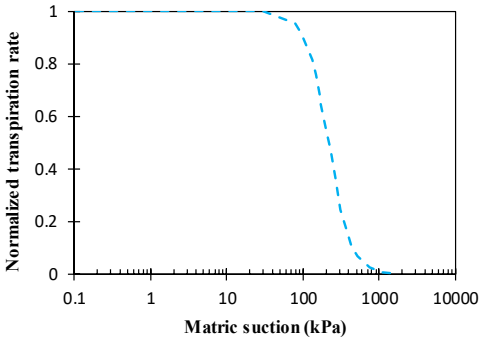

Fig. 3. Normalized transpiration rate of Schefflera [31]

Fig. 4 illustrates the normalized root density distribution of Schefflera heptophylla. In order to calculate the normalized water uptake distribution (π'_{root}) in equation (3), this curve should be used to measure the amount of water uptake by roots along the soil depth. Normalized root density from 0.46 at the surface is increased to 1.0 at a normalized depth of 0.4 and is decreased to 0.2 at a normalized depth of 1.0 [31].

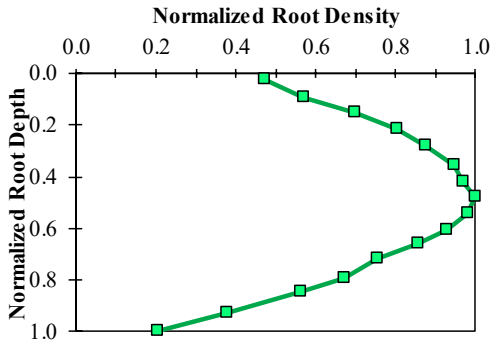

Fig. 4. Normalized distribution of root density [31]

2.3 Soil properties

The type of soil modeled in this study is completely decomposed granite soil (CDG). This soil contains 19% gravel, 42% sand, 27% silt, and 12% clay. According to the Unified Soil Classification System, this soil is classified as silty sand [11]. As vegetation changes the hydraulic and mechanical properties of the soil, two types of bare and vegetated soils were investigated in this study. The differences arise from cohesion, permeability, and the soil-water retention properties. The hydraulic conductivity of the bare and vegetated soil is 2.16×10^{-6} m/s, and 1.2×10^{-6} m/s, respectively [22]. According to the experimental literature, Fig. 5 shows the soil water retention curve (SWRC) of bare and vegetated soil [12]. However, no definitive coefficients in regulations have been defined for this issue due to the conflicting results.

The cohesion of the rooted soil consists of two components [6]:

$$C = C_S + C_R \quad (4)$$

where C_S is the cohesion of bare soil, and C_R is additional cohesion by roots. However, according to recent research, additional cohesion of this plant specie varies from 12-30 kPa [32]. The average value of 20 was hence selected for the vegetated soil because the cohesion of bare soil is zero [4, 33]. The effective friction angle of CDG at critical state is 37.4 degree [4]. According to a recent study, a slight increase in the friction angle of vegetated soil was reported by comparing the triaxial test performed on bare and rooted soil samples [5]. Therefore, the effect of vegetation on soil friction angle was ignored in this study. Other properties of the CDG are summarised in Table 3. It is noted that the influence of dissolved salts on soil properties were ignored because of the simplicity [34, 35]. It is also assumed that vegetation has minor effects on dilation rate during shearing process [36].

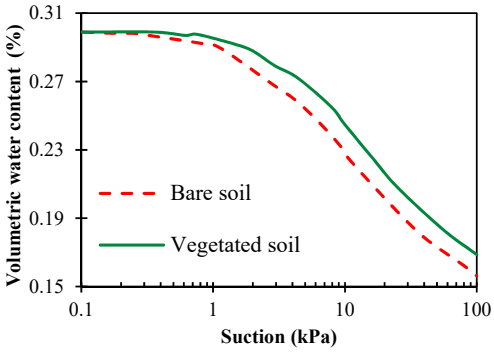

Fig. 5. SWRCs of bare and vegetated soils [12]

Table 3. Physical properties of the CDG

Parameters	Vegetated soil	Bare soil	Reference
γ: kN/m³	20	20	[25]
G_s	2.59	2.59	
c': kPa	20	0	[4]
ϕ_{cr}	37.4	37.4	
k_s :m/s	1.2×10^{-6}	2.16×10^{-6}	[22]

2.4 Geometry and boundary conditions

Two slopes with different conditions were considered to compare the vegetation effect on the hydro-mechanical properties of shallow failures. Fig. 6 shows the geometry and boundary conditions of bare and vegetated slopes. The height and angle of the slopes are 8 m and 40 degrees, respectively. The initial water table is located at the bottom on the right side and 5 meters deep from the surface on the left side. The bare slope is modeled homogenously bare, but the vegetated slope comprises two soil layers; a vegetated layer in the surface with 0.5m thickness seated on the bare layer. As shown in Fig. 6, the hydraulic boundary conditions in the bottom and sides of the slopes are considered impermeable. On the surface of the two models, the land-climate interaction boundary is applied to simulate the effect of climate conditions and vegetation. Land-climate interaction boundary contains temperature, precipitation, relative humidity, solar radiation, and wind speed which calculate the evapotranspiration of bare and vegetated slope by equation (2). As a result, the calculated the evapotranspiration is equal 0.27 mm/day.

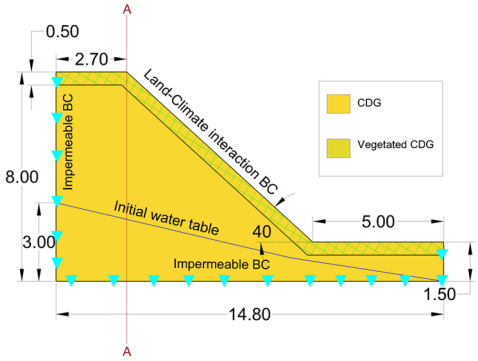

Fig. 6. Geometry and boundary condtion

3 Interpretation of the Results

3.1 Effect of vegetation on hydraulic properties

Fig. 7 compares the pore water pressure distribution of bare (Fig. 7-a) and vegetated (Fig. 7-b) slopes along the soil depth at the A-A section for the HI scenario. In the initial condition, the distribution of pore water pressure changes linearly along the depth. After raining for ten days, suction dropped to zero kPa in the bare slope, as shown in Fig. 7-a. On the other hand, Fig. 7-b. shows that in the vegetated slope, after ten days of rainfall, there is still matric suction along the soil depth. As mentioned above, the hydraulic conductivity of vegetated soil is lower than bare soil, and rainfall infiltration of the vegetated slope is less than the bare slope. Hence, surface runoff prevails the infiltration. Furthermore, root water uptake causes a decrease in volumetric water content, and hence a rise in matric suction.

Fig. 8 compares the pore water pressure distribution of vegetated and bare slopes along the soil depth before and after rainfall at the A-A section for the LI scenario. During rainfall events, due to rainfall infiltration, pore-

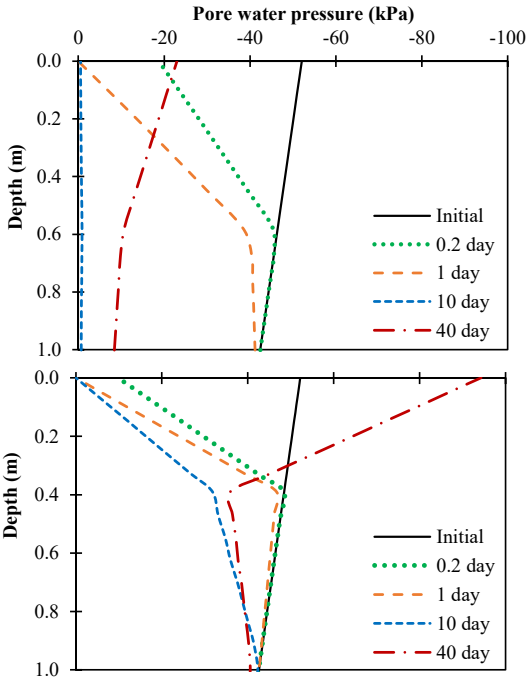

Fig. 7. Distribution of pore water pressure along A-A section in HI scenario for: a) bare slope, and b) vegetated slope

water pressure increases. After 20 days of precipitation, pore water pressure in the bare slope reaches zero kPa, but there is still matric suction in the vegetated slope. After drying for one month, on the 50th day, matric suction in the bare and vegetated soil becomes 22 and 62 kPa, respectively. The results also confirm that the influence zone of rainfall reduces with depth significantly [37].

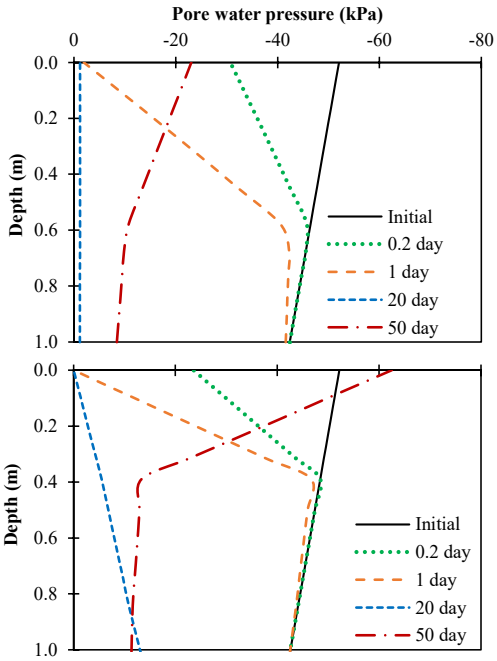

Fig. 8. Distribution of pore water pressure along depth in LI scenario for: a) bare slope, and b) vegetated slope

By comparing the results of Fig. 7 and Fig. 8, there is no difference between the matric suction of the two rainfall scenarios in the bare slope, right after rainfall and after one month of drying. However, in vegetated slopes, the final matric suction in the HI scenario is about 1.5 times greater than the LI scenario. The difference between the matric suction in the two rainfall scenarios in the vegetated slope was that the volumetric water content after LI rainfall was higher than in the HI rainfall scenario. In other words, Fig. 9 indicates that in the LI scenario, the soil after rainfall was nearer to the saturated condition (θ_s = 0.3), but in the HI scenario, there is still suction, especially in the rooted zone [38]. Therefore, after 30 days of drying, the matric suction in the HI scenario was higher than that of the LI one. Thus, due to the lower hydraulic conductivity, penetration is reduced and surface runoff occurs. As a result, long-term rainfalls, even with low intensity, are more critical for shallow landslides.

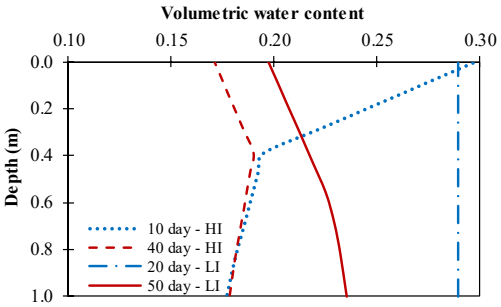

Fig. 9. Distribution of volumetric water content for vegetated slope in LI and HI scenarios

3.2 Effect of vegetation on slope stability

Fig. 10 indicates the variations in the factor of safety with time for the two rainfall scenarios. The factor of safety in both cases of the bare and vegetated slope in either scenario is decreased due to rainfall infiltration and reduction of soil strength. The reduction in the safety factor in the bare slope is more than in the vegetated slope during rainfall.

In bare slopes, as shown in Fig. 10, in the HI rainfall, the safety factor reduction is more than in LI rainfall. By comparing the two scenarios, the most critical condition is related to the HI rainfall, with the lowest factor of safety (i.e., 1.06). Although the rainfall duration in the LI scenario was longer, the rainfall intensity had more significant effect on the stability of the bare slopes. In the LI scenario, the drainage rate is greater than or equal to the precipitation rate, and the saturation process cause zero suction in 20 days, but in the HI scenario, the rain induces zero suction in 10 days. So the factor of safety reduces faster in the HI scenario than in the LI scenario.

In vegetated slopes, the safety factor is decreased during the rainfall, but the safety factor reduction was less than in the case of bare slope. Because the vegetated slope has a greater ability to maintain suction and soil strength during rainfalls, especially in HI rainfall. In the case of LI rainfall, the reduction in the factor of safety is more significant than HI rainfall. As discussed in the last sections, plants had better performance in high-intensity and short-term rainfalls. As shown in Fig. 10, the factor of safety right after rainfall was 1.61. Therefore, the rainfall duration had a greater effect on the stability of the vegetated slope. In conclusion, the bare slopes are more vulnerable to short-term, high-intensity rainfall, and slope stability would be enhanced by planting on slopes. The factor of safety of the vegetated slope is higher than the bare slope due to the higher matric suction and additional cohesion created by the roots.

After rainfall for all cases, in the drying process, due to evaporation or evapotranspiration, the volumetric water content in the soil decreased [39], matric suction increased, and the safety factor increased.

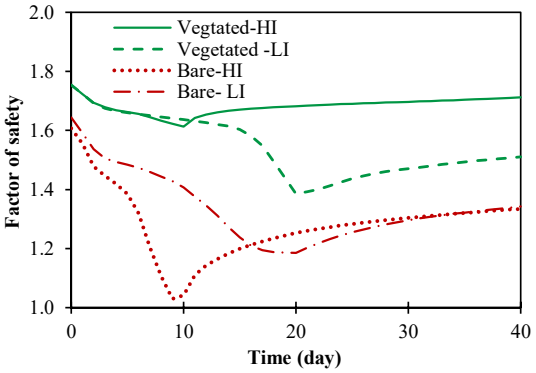

Fig. 10. Effect of vegetation and rainfall on factor of safety in LI and HI scenarios

4 Conclusions

In this study, the effect of the Schefflera heptophylla tree on the slope stability subjected to rainfall was investigated numerically. Two slopes with the same geometry, but one with vegetation and another one without it, were subjected to two rainfall intensities. The corresponding hydraulic and mechanical properties of vegetated and bare soils, were retrieved from the literature. Some key findings are reported accordingly:

1. During the rainfall due to water infiltration, matric suction in both scenarios decreased. In the vegetated slope during the rainfall event, the calculated matric suction is higher than the bare slope. Because the presence of vegetation due to root occupancy and root water uptake reduces the hydraulic conductivity of the soil.
2. The suction increased after the rainfall due to evaporation and transpiration. As a result, the matric suction at the slope surface with vegetation is greater than that of the bare slope. After the rainfall of 40 mm/day, while evaporation was in progress, the matric suction of the vegetated slope at the surface is approximately four times greater than the bare slope. However, in 20 mm/day rainfall, the matric suction is about threefold.
3. Planting on slopes would improve slope stability by reducing the vulnerability of bare slopes to high-intensity rainfall. Because of the higher matric suction and additional cohesion induced by the root system, the vegetated slope has a higher safety factor than the bare slope.

4. Low-intensity rainfall reduces the factor of safety in the vegetated slope more than HI rainfall. It is therefore postulated that plants performed better in high-intensity rainfall.
5. Based on the results, the use of vegetation for stabilizing slopes has the potential to be effective in Rasht, Iran, where the climate and rainfall data were obtained. It is noted that advanced constitutive models related to unsaturated soils will provide better insight into the soil-climate interactions [40].

Acknowledgments

The financial support provided by Iran National Science Foundation for "Experimental study of the hydro-mechanical behaviour of rooted soils in green stabilization of unsaturated slopes" by way of grant 4000730 is gratefully acknowledged. In addition, the authors are grateful to Iran's National Elites Foundation for supporting this research through the "Dr. Kazemi-Ashtiani Award."

References

1. S. Sadat Naseri, H. Sadeghi, and A. Garakani, Sharif J. Civ. Eng., **38**, 51-61 (2022)
2. A. Garakani, M. M. Birgani, and H. Sadeghi, Bull. Eng. Geol. Environ., **80**, 7525–7549 (2021)
3. H. Sadeghi, and C.W.W. Ng, 7th Int. Conf. unsaturated soils (2018)
4. C. W. W. Ng, V. Kamchoom, and A. K. Leung, Landslides, **13**, 925-938 (2016)
5. H. Rahardjo, A. Satyanaga, E. C. Leong, V. A. Santoso, and Y. S. Ng, Soils Found., **54**, 417-425 (2014)
6. D. Petley, Geology, **40**, 927-930 (2012)
7. J. P. Turner, and W. G. Jensen, J. Geotech. Geoenvironmental Eng., **131**, 141-150 (2005)
8. M. T. Löbmann, C. Geitner, C. Wellstein, and S. Zerbe, Earth-Sci. Rev, 209 (2020)
9. N. K. Kokutse, A. G. T. Temgoua, and Z. Kavazović, Ecol. Eng., **86**, 146-153 (2016)
10. W. Wu, B.M. Switala, M.S. Acharya, R. Tamagnini, M. Auer, F. Graf, L. te Kamp, and W. Xiang, Geomech. Geoengin.,163-177 (2015)
11. C. W. W. Ng, J. J. Ni, A. K. Leung, C. Zhou, and Z. J. Wang, Geotechnique, **66**, 711-724 (2016)
12. C. W. W. Ng, J. J. Ni, and A. K. Leung, Geotechnique, **70**, 867-881 (2020)
13. C. W. W. Ng, K. X. Woon, A. K. Leung, and L. M. Chu, Ecol. Eng., **52**, 219-223 (2013)
14. C. W. W. Ng, A. K. Leung, and K. X. Woon, Can. Geotech. J., **51**, 311-321 (2014)
15. H. Guo, X. Chen, D. Song, Q. Mu, H.Sadeghi, H. Jiang, and M. Lv, J. Mt. Sci. (2023)
16. H. Sadeghi and P. AliPanahi, Eng. Geol., **278**, 105827 (2020).
17. A. Hedayati-Azar, and H. Sadeghi, J. Contam. Hydrol., **249**, 104042 (2022)
18. A. Jotisankasa, and T. Sirirattanachat, Can. Geotech. J., **54**, 1612-1622 (2017)
19. J. Ni, C. W. W. Ng, and Y. Gao, J. Theor. Biol., **484**, 110019 (2020)
20. C. W. W. Ng and A. K. Leung, J. Geotech. Geoenvironmental Eng., **138**, 58-68 (2012)
21. M. Ghestem, R. C. Sidle, and A. Stokes, Bioscience, **61**, 869-879 (2011)
22. A. K. Leung, D. Boldrin, T. Liang, Z. Y. Wu, V. Kamchoom, and A. G. Bengough, Geotechnique, **68**, 646-652 (2018)
23. A. K. Leung, A. Garg, and C. W. W. Ng, Eng. Geol., **193**,183-197 (2015)
24. B. M. Switała, and W. Wu, Geotechnique, **68**, 481-491 (2018)
25. H. Sadeghi, A. Kolahdooz, and M. M. Ahmadi, Rock Soil Mech., **43**, 2136 (2022)
26. A. Garg, and C. W. W. Ng, J. Plant Nutr. Soil Sci., **178**, 586-591 (2015)
27. J. Ni, Y. Cheng, Q. Wang, C. W. W. Ng, and A. Garg, J. Hydrol., **571**, 494-502 (2019)
28. H. Zhu, L. M. Zhang, T. Xiao, and X. Y. Li, Comput. Geotech., **85**, 84-89 (2017)
29. S. K. Vanapalli, D. G. Fredlund, D. E. Pufahl, and A. W. Clifton, Can. Geotech. J., **33**, 379-392 (1996)
30. R. A. Feddes, H. Hoff, M. Bruen, T. Dawson, P. De Rosnay, P. Dirmeyer, R.B. Jackson, A. Kleidon, A. Lilly and A. J. Pitman, BAMS, **82**, 2797-2810 (2001)
31. A. Garg, A. K. Leung, and C. W. W. Ng, Catena, **135**, 78-82 (2015)
32. J. J. Ni, A. K. Leung, and C. W. W. Ng, Landsc. Ecol. Eng., **15**, 223-230 (2019)
33. C.W.W. Ng, H. Sadeghi and F. Jafarzadeh, Can. Geotech. J., **54(5)**, 690–699 (2016)
34. H. Sadeghi and H. Nasiri, Geotech. Lett., **11**, 21–29 (2021)
35. H. Sadeghi, S.K. Hossen, C.F. Chiu, Q. Cheng and C.W.W. Ng, Jpn. Geotech. Soc. Spec. Publ., **HKG-04**, 221–225 (2016)
36. C.W.W. Ng, H. Sadeghi, F. Jafarzadeh, M. Sadeghi, C. Zhou and S. Baghbanrezvan, Can. Geotech. J., **57(2)**, 221–235 (2020)
37. H. Sadeghi, A.C.F. Chiu, C.W.W. Ng and F. Jafarzadeh, Sci. Iran., **27(2)**, 596–606 (2020)
38. A. Bazargan, H. Sadeghi, R. Garcia-Mayoral and G. McKay, Sci. Total Environ., **450**, 127–134 (2015)
39. C.W.W. Ng, H. Sadeghi, S.K. Hossen, C.F. Chiu, E.E. Alonso and S. Baghbanrezvan, Can. Geotech. J., **53(8)**, 1258–1269 (2016)
40. M. Vahdani, M.M. Hajitaheriha, A. Hasani Motlagh and H. Sadeghi, Indian Geotech. J., **52**, 865–876 (2022)